# $Sr_{2-x}Ba_xCuO_2(CO_3)$: A Series of Antiferromagnetic Layered Oxide Carbonates

**Alexandros Lappas and Kosmas Prassides***

School of Chemistry and Molecular Sciences, University of Sussex, Brighton BN1 9QJ, U.K.

**A. Robert Armstrong**

Rutherford Appleton Laboratory, Didcot, Oxon OX11 0QX, U.K.

**Peter P. Edwards***

School of Chemistry, University of Birmingham, Birmingham B15 2TT, U.K.

*Received September 15, 1992*

All superconducting copper oxide systems have in common the presence of $(CuO_2)_\infty$ layers which form part of strongly elongated octahedral[1] $CuO_6(La_{2-x}Sr_xCuO_{4-\delta})$, square-pyramidal[2] $CuO_5$-$(Nd_{2-x-y}Ce_xSr_yCuO_{4-\delta})$, or square-planar[3] $CuO_4(Nd_{2-x}Ce_xCuO_{4-\delta})$ units. The undoped parent materials in which the formal Cu oxidation state is equal to +2 are characterized by the presence of strong antiferromagnetic (AF) correlations.[4,5] An intimate relation exists between the magnetic and (super)conducting properties of the $CuO_2$ layers, as the AF long-range order (LRO) is *always* removed upon electron-[5] or hole-doping[4] *before* the onset of superconductivity. Recently, it has been demonstrated that hole doping of the oxide carbonate $Sr_2CuO_2(CO_3)$, which also contains infinite $CuO_2$ layers,[6] leads to superconductivity at ~40 K.[7] $Sr_2CuO_2(CO_3)$ differs structurally from $La_2CuO_4$ in that the $CuO_6$ octahedra present are so severely elongated that the compound may be regarded as consisting of alternating structural motifs of $CuO_2^{2-}$ sheets and $Sr_2(CO_3)^{2+}$ slabs.[6d] However, the presence of bridging oxygens between Cu and C appears to be crucial in determining how this compound[6c,6d] will be doped, leading to hole superconductivity.[7] In this communication, we report that ordered local magnetic moments appear at the $Cu^{2+}$ sites in $Sr_2CuO_2(CO_3)$ and its solid solutions with $Ba^{2+}$. This points once again to the importance of strong correlations and the need to understand the competition between magnetism and superconductivity in any model for the high-$T_c$ cuprates.

$Sr_{2-x}Ba_xCuO_2(CO_3)$ compositions ($0 \le x \le 2$) were synthesized by standard solid state reactions, as reported earlier.[6d] For compositions involving greater than 50% Sr and for the pure Ba compound, the reactions were performed exclusively under enclosed conditions; for compositions with less than 50% Sr, the samples were fired first in air before the final treatment under enclosed conditions. X-ray powder diffraction profiles at room temperature were recorded on a Philips PW1050 diffractometer. Powder neutron diffraction measurements were performed between 5 and 300 K with the high-intensity medium-resolution D1B diffractometer[8] at the Institut Laue Langevin, Grenoble, France, using neutrons with a mean wavelength of 2.522 Å. Data were recorded for the $x = 0$, 0.5, 1.35, and 1.5 samples for $2\theta \sim$ 10–90° in steps of 0.2°.

The gross structural details of $Sr_2CuO_2(CO_3)$ were described in earlier work.[6] The structure is tetragonal, consisting of alternating $CuO_2$ and $Sr_2CO_3$ layers. However, the exact location and associated orientational ordering of the carbonate groups proved more difficult to decipher. Preliminary evidence for O sharing between Cu and C atoms came from time-of-flight powder neutron diffraction studies,[6d] but the $CO_3$ groups were found to be orientationally disordered. More recent work[6e] has confirmed the O sharing between the Cu and C atoms; however, it also identified the presence of a superstructure (space group $I\bar{4}$), resulting from ordering of the carbonate groups (Figure 1). With a standard Rietveld–Hewat profile refinement program and the above structural model, our medium resolution data refine satisfactorily in the $I\bar{4}$ tetragonal space group for all the $Sr_{2-x}Ba_xCuO_2(CO_3)$ compositions studied and at all temperatures between 5 K and room temperature. The average $R$ factors[9] over the full temperature range obtained in the refinements, e.g. of the $Sr_{1.5}Ba_{0.5}CuO_2(CO_3)$ profiles,[10] are as follows: $R_{wp} = 6.1\%$, $R_p = 4.5\%$, $R_e = 1.2\%$. The $CuO_2$ layers appear to remain strictly tetragonal with no evidence of any structural distortion. The smooth temperature evolution of the unit cell volume of the samples with $x = 0$, 0.5, and 1.35 is shown in Figure 2.

Figure 3 shows the normalized expansion in the intra- and interlayer spacings relative to the $Sr_2CuO_2(CO_3)$ end member upon (Sr, Ba) solid solution formation. Both the intralayer $a$ and the interlayer $c$ dimensions are normalized to the difference in

* To whom correspondence should be addressed.

(1) (a) Day, P.; Rosseinsky, M. J.; Prassides, K.; David, W. I. F.; Moze, O.; Soper, A. K. *J. Phys. C* **1987**, *20*, L429. (b) Paul, D. M.; Balakrishan, G.; Bernhoeft, N. R.; David, W. I. F.; Harrison, W. T. A. *Phys. Rev. Lett.* **1987**, *58*, 1976. (c) Jorgensen, J. D.; Schuttler, H. B.; Hinks, D. G.; Capone, D. W.; Zhang, K.; Brodsky, M. B.; Scalapino, D. J. *Phys. Rev. Lett.* **1987**, *58*, 1024. (d) Cava, R. J.; Santoro, A.; Johnson, D. W.; Rhodes, W. W. *Phys. Rev. B* **1987**, *35*, 6716.

(2) Sawa, H.; Suzuki, S.; Watanabe, M.; Akimitsu, J.; Kolcirlo, K.; Asaio, H.; Izuki, F.; Takayama-Muromachi, E. *Nature* **1989**, *337*, 347.

(3) (a) Tokura, Y.; Takagi, H.; Uchida, S. *Nature* **1989**, *337*, 345. (b) Singh, K. K.; Ganguly, P.; Rao, C. N. R. *Mater. Res. Bull.* **1982**, *17*, 493. (c) Rosseinsky, M. J.; Prassides, K.; Day, P. *Physica C* **1989**, *161*, 21. (d) Lightfoot, P.; Richards, D. R.; Dabrowski, B.; Hinks, D. G.; Pei, S.; Marx, D. T.; Mitchell, A. W.; Zheng, Y.; Jorgensen, J. D. *Physica C* **1990**, *168*, 627. (e) Rosseinsky, M. J.; Prassides, K. *Europhys. Lett.* **1991**, *14*, 551.

(4) (a) Vaknin, D.; Sinha, S. K.; Moncton, D. E.; Johnston, D. C.; Newsam, J.; Safinya, C. R.; King, H. *Phys. Rev. Lett.* **1987**, *58*, 2802. (b) Freltoft, T.; Shirane, G.; Mitsuda, S.; Remeika, J. P.; Cooper, A. S. *Phys. Rev. B* **1988**, *37*, 137. (c) Birgeneau, R. J.; Kastner, M. A.; Aharony, A. *Z. Phys. B* **1988**, *71*, 57. (d) Rosseinsky, M. J.; Prassides, K.; Day, P. *J. Mater. Chem.* **1991**, *1*, 597.

(5) (a) Rosseinsky, M. J.; Prassides, K.; Day, P. *J. Chem. Soc., Chem. Commun.* **1989**, 1734. (b) Rosseinsky, M. J.; Prassides, K. *Physica C* **1989**, *162*, 522. (c) Rosseinsky, M. J.; Prassides, K. *Physica B* **1990**, *165*, 1187. (d) Rosseinsky, M. J.; Prassides, K.; Day, P. *Inorg. Chem.* **1991**, *30*, 2680. (e) Rosseinsky, M. J.; Prassides, K.; Scott, C. A. *Inorg. Chem.* **1991**, *30*, 3367. (f) Rosseinsky, M. J.; Prassides, K.; Scott, C. A. *J. Magn. Magn. Mater.* **1992**, *104*, 599. (g) Rosseinsky, M. J.; Prassides, K. *Physica B* **1992**, *180*, 408. (h) Endoh, Y.; Matsuda, M.; Yamada, K.; Kakurai, K.; Hidaka, Y.; Shirane, G.; Birgeneau, R. J. *Phys. Rev. B* **1989**, *40*, 7023. (i) Matsuda, M.; Yamada, K.; Kakurai, K.; Kadowski, H.; Thurston, T. R.; Endoh, Y.; Hidaka, Y.; Birgeneau, R. J.; Gehring, P. M.; Moudden, A. H.; Shirane, G. *Phys. Rev. B* **1990**, *42*, 10098. (j) Skanthakumar, S.; Zhang, H.; Clinton, T. W.; Li, W.-H.; Lynn, J. W.; Fisk, Z.; Cheong, S. W. *Physica C* **1989**, *160*, 124. (k) Luke, G. M.; et al. *Phys. Rev. B* **1990**, *42*, 7981.

(6) (a) von Schnering, H. G.; Hartweg, M.; Walz, L.; Popp, T.; Becker, T.; Schwarz, *Jahresbericht des MPI für Festkörperforschung Stuttgart*, MPI für Festkörperforschung: Stuttgart, Germany, 1988; p 94. (b) Müller-Buschbaum, H. *Angew. Chem.* **1989**, *28*, 1472. (c) Babu, T. G. N.; Fish, D. J.; Greaves, C. *J. Mater. Chem.* **1991**, *1*, 677. (d) Armstrong, A. R.; Edwards, P. P. *J. Solid State Chem.* **1992**, *98*, 432. (e) Miyazaki, Y.; Yamane, H.; Kajitani, T.; Oku, T.; Hiraga, K.; Morii, Y.; Fuchizaki, K.; Funahashi, S.; Hirai, T. *Physica C* **1992**, *191*, 434.

(7) Kinoshita, K.; Yamada, T. *Nature* **1992**, *357*, 313.

(8) Pannetier, J. *Chem. Scr. A* **1986**, *26*, 131.

(9) Rietveld, H. M. *J. Appl. Crystallogr.* **1969**, *2*, 65.

(10) The average number of observables used in the Rietveld analyses was 220; 14 Bragg reflections were included and 14 structural and instrumental variables refined.

0020-1669/93/1332-0383$04.00/0 

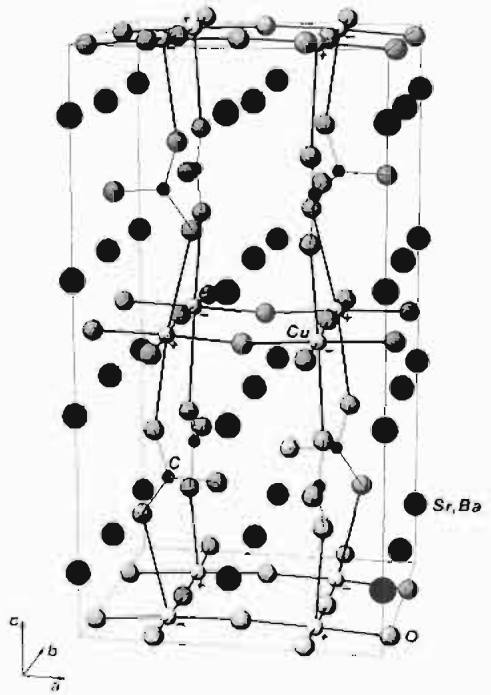


**Figure 1.** Magnetic and crystal structure of $Sr_{2-x}Ba_xCuO_2(CO_3)$. (+) and (−) symbols at $Cu^{2+}$ sites indicate antiparallel spins.

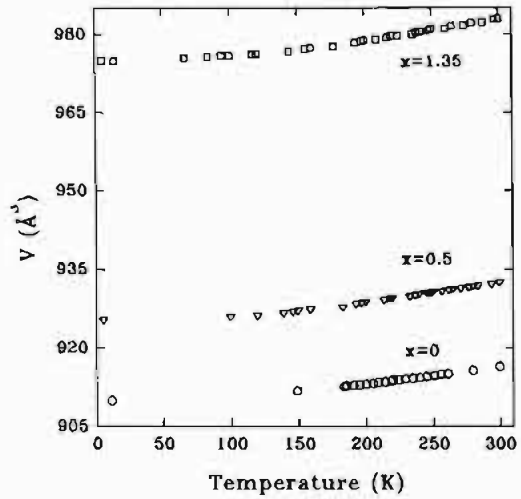


**Figure 2.** Unit cell volume of $Sr_{2-x}Ba_xCuO_2(CO_3)$ ($x$ = 0, 0.5, 1.35) plotted as a function of temperature.

ionic radii between the eight-coordinate $Ba^{2+}$ and $Sr^{2+}$ ions. Vegard's law for ideal solid solution formation is exhibited by the evolution of the interlayer spacing as the $Ba^{2+}$ doping level increases.[11] The effect of the change in radius of the alkaline-earth metal ion is more indirect on the basal plane lattice dimensions where the strong Cu–O bonding is present. In the Sr-rich part of the diagram, the size of the basal plane still increases linearly,[12] *albeit* at a smaller rate than the interlayer spacing. However, in the Ba-rich part, where oxidizing preparative conditions were employed, deviations from linearity are apparent, indicating disruption of the $CuO_2$ layers; a much smaller anomaly may be present in the interlayer expansion. Our medium resolution data cannot distinguish between the various possibilities which may give rise to this effect—we note though that two possible reasons are likely to give rise to this behavior: (i) the alkaline-earth metal ions may substitute on the copper sites, as

(11) A least-squares fit of the normalized interlayer spacing to a straight line results in a slope equal to 0.74(1), with a value of 1 expected if the lattice expansion was wholly due to the larger size of $Ba^{2+}$.
(12) The slope of the line fitted to the basal plane dimension in the Sr-rich part is 0.15(1).

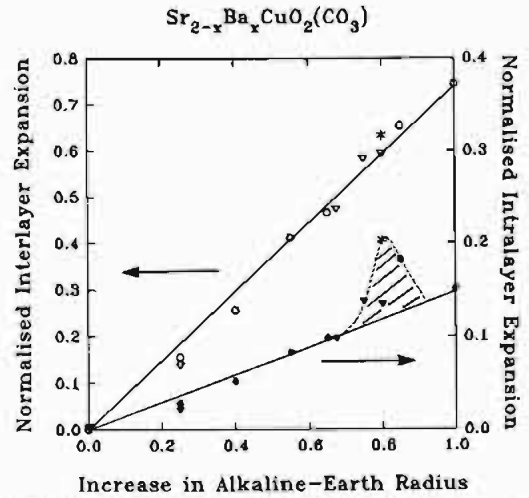


**Figure 3.** Variation of the normalized intralayer and interlayer expansion in the $Sr_{2-x}Ba_xCuO_2(CO_3)$ series relative to the $Sr_2CuO_2(CO_3)$ parent member as a function of the normalized change in ionic size of the alkaline-earth metal spacer at room temperature. The shaded region corresponds to samples prepared under oxidizing conditions. [Key to symbols: (○) X-ray (present study); (▽) neutron diffraction data (present study); (✱) data from ref 13].

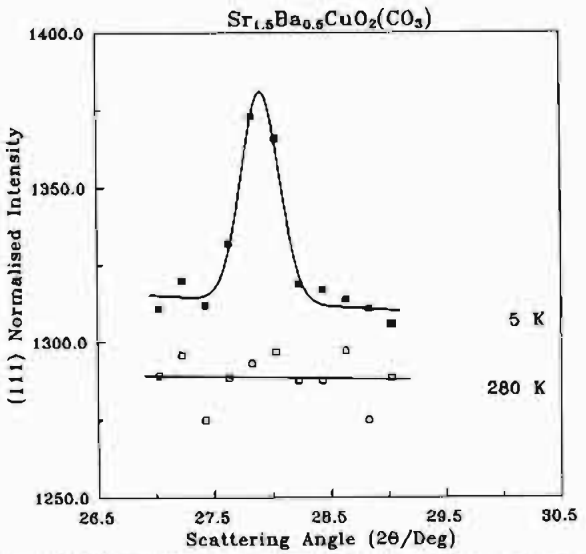


**Figure 4.** Powder neutron diffraction profile of $Sr_{1.5}Ba_{0.5}CuO_2(CO_3)$ between 26.5 and 29.5° at 5 and 280 K. The peak is not evident at 280 K, which is above $T_N$.

has been found[13] for the related system $Ba_4CaCu_{2.24}O_{6.96}(CO_3)_{0.5}$ and/or (ii) excess oxygen may be accommodated in the structure (cf. the existence of oxygen-rich[14] ternary alkaline-earth metal cuprates $Ba_2CuO_{3+\delta}$). No anomaly is apparent for the $x$ = 2 sample, which was prepared in a reducing atmosphere.

Close inspection of the room temperature and the 5 K powder diffraction profiles of $Sr_{2-x}Ba_xCuO_2(CO_3)$ ($x$ = 0, 0.5, and 1.35) revealed the presence of a weak peak in the vicinity of $2\theta \sim 28°$ (Figure 4). The magnetic origin of the peak is confirmed by the evolution of its intensity with temperature (Figure 5). It could be also readily indexed on the basis of the chemical unit cell as $(111)_M$, implying that the magnetic unit cell coincides with the chemical one ($a_M = a$, $c_M = c$, $k = 0$) and the magnetic moments of the copper ions, related by the body-centring translation vector $\tau = (1/2, 1/2, 1/2)$ are aligned oppositely. The AF ordering is thus of G-type[15] and is illustrated in Figure 1. It proved impossible to identify any more magnetic reflections as the presence of the

(13) Greaves, C.; Slater, R. P. *J. Mater. Chem.* **1991**, *1*, 17.
(14) de Leeuw, D. M.; Mutsaers, C. A. H. A.; Langereis, C.; Smoorenburg, H. C. A.; Rommers, P. J. *Physica C* **1988**, *152*, 39.

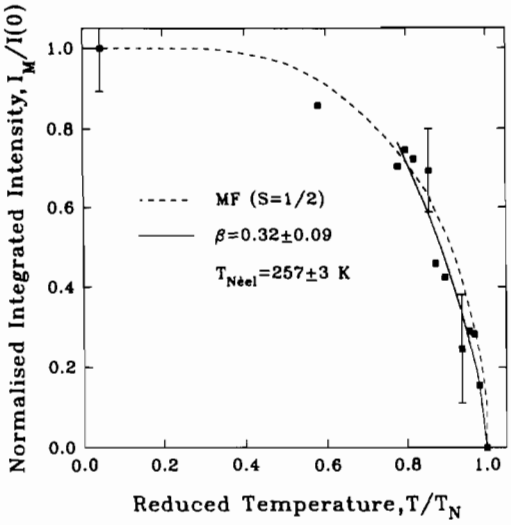


**Figure 5.** Temperature dependence of the normalized Cu sublattice magnetization in $Sr_2CuO_2(CO_3)$. The solid line represents a fit, close to the transition temperature, to the expression for critical behavior: $I_M/I(0) = (1 - T/T_N)^{2\beta}$, with $\beta = 0.32(9)$ and $T_N = 257(3)$ K. The dashed curve represents the calculated mean-field curve for a $S = {}^1/_2$ system.

(expected) weaker $(113)_M$ and $(115)_M$ was masked by the very intense $(004)_N$ and $(222)_N$ nuclear peaks. No evidence for any magnetic scattering was found for the $Sr_{0.5}Ba_{1.5}CuO_2(CO_3)$ composition which lies within the shaded region of Figure 3; both excess oxygen (Cu oxidation states >+2) and/or alkaline-earth metal substitution of copper sites will destroy the Néel state.

The magnetic structure of $Sr_{2-x}Ba_xCuO_2(CO_3)$ contains AF $CuO_2$ layers identical to the ones observed in $(Ca_{0.85}Sr_{0.15})CuO_2$,[16] $La_2CuO_4$,[4] $Nd_2CuO_4$,[5] and $YBa_2Cu_3O_6$.[17] Furthermore, adjacent layers are also coupled antiferromagnetically. In uniaxial systems, powder diffraction cannot lead to unambiguous determination of the magnetic moment direction; only the angle between the spin direction and the unique ($c$) axis can be determined.[18] For illustrative purposes, we considered two models for the spin orientation: along the c axis ($\parallel$) and in the plane ($\perp$). However, $(111)_M$ is the strongest magnetic peak expected whether the moment is parallel or perpendicular to the $c$ axis. Thus in the present case, the spatial orientation of the magnetic moment cannot be uniquely determined. In order to estimate the magnitude of the ordered Cu magnetic moment, we used[19]

$$I_M = CF_M^2 m_{111}/(\sin\theta \sin 2\theta) \qquad (1)$$

normalized with respect to the structure factors of the $(002)_N$ and the $(004)_N$ nuclear reflections. $m_{111}$ is the multiplicity of the $(111)_M$ peak with the magnetic structure factor given by[19] $F_M \approx 8.0\gamma_0 Sf(\mathbf{q})\langle q\rangle$, where $\langle q\rangle$ is the magnetic interaction term, $\gamma_0$ the gyromagnetic ratio of the neutron, and S the $Cu^{2+}$ spin. The antiferromagnetic form factor $f(\mathbf{q})$ for Cu was obtained by interpolation from the measurements of Freltoft et al.[4b] The average magnetic moment per Cu ion at 5 K is thus estimated to be $\mu_\parallel = (0.40 \pm 0.02)\ \mu_B$ and $\mu_\perp = (0.50 \pm 0.02)\ \mu_B$ for parallel and perpendicular orientations for $Sr_2CuO_2(CO_3)$[20] and $\mu_\parallel = (0.28 \pm 0.02)\ \mu_B$ and $\mu_\perp = (0.35 \pm 0.02)\ \mu_B$ for $Sr_{1.5}Ba_{0.5}CuO_2(CO_3)$, respectively.[21]

The temperature evolution of the normalized integrated intensity, $I_M/I(0)$, of the $(111)_M$ peak (Figure 5) is characteristic of a continuous transition. Near the ordering temperature, the intensity was fitted to the equation $I_M = I(0)(1 - T/T_N)^{2\beta}$. The critical exponent analysis in the 200–260 K temperature range for $Sr_2CuO_2(CO_3)$ gave $\beta = 0.32 \pm 0.09$ and $T_N = 257 \pm 3$ K. (The Néel temperature of the $x = 0.5$ sample is estimated to be $240 \pm 5$ K.) This result favors a 3D spin Hamiltonian close to the transition (Ising models, $\beta = 0.325, 0.345$; Heisenberg model, $\beta = 0.365$) but excludes a mean-field model.[22] The strong superexchange interactions between the $Cu^{2+}$ ions and the bridging equatorial $O^{2-}$ ions are principally responsible for the AF order exhibited by this series of oxide carbonates. The interlayer exchange interactions are crucial in inducing the 3D LRO by coupling the essentially 2D AF $Cu^{2+}$ sublattices. Even though successive $CuO_2$ layers are separated by ~7.5–7.8 Å, the interlayer interactions are considerably enhanced by the presence of the bridging $CO_3^{2-}$ groups which lead to a pseudooctahedral coordination for Cu. A crude estimate of the interlayer exchange constant, $J_\perp \sim 2$ K, can be deduced if we assume that 3D LRO occurs when[23] $k_B T_N \sim J_\perp(\xi_{2D}/a_{Cu-Cu})^2$, where $\xi_{2D}$ is the correlation length and $a_{Cu-Cu}$ is the Cu–Cu separation in the layers. The values of the Cu magnetic moment, $\mu \sim 0.3$–$0.5\ \mu_B$, obtained in this series are comparable to those obtained for other parent members of layer cuprate superconductors.[4,5,16,17] They display a marked reduction from 1.14 $\mu_B$ predicted from $S = {}^1/_2$ and $g = 2.28$ for $Cu^{2+}$ due to zero-point spin fluctuations and strong covalency. The in-plane Cu–O bond lengths in the present series (≥1.95 Å) are comparable with the ones found in $Nd_2CuO_4$ (Cu coordination number 4; 1.9585 Å), but considerably larger than the ones in $La_2CuO_4$ (Cu coordination number 6; 1.9036 Å). Longer Cu–O bond lengths imply reduced transfer integrals and reduced covalency. The similarity in the measured moments may thus reflect a balance between covalency and quantum fluctuation effects associated with low dimensionality. The slight reduction in the Cu moment with increased $Ba^{2+}$ concentration may thus arise from an increased importance of spin fluctuations, as a result of the increased 2D character upon interlayer expansion, despite the reduced covalency, associated with a slight in-plane expansion.

In conclusion, we have shown that ordered local magnetic moments appear at the $Cu^{2+}$ sites of $Sr_{2-x}Ba_xCuO_2(CO_3)$, the parent of a new series of hole-doped superconductors.[7] Although there are differences in the details of the magnetic structures, similar magnetic behavior is exhibited by the parent members of all the families of the high-$T_c$ cuprates;[4,5,16,17] a universal picture is thus emerging of a Mott–Hubbard description of strongly correlated $\sigma^*$ electrons in the layers with magnetic LRO disappearing upon doping, before the onset of metallic and superconducting behavior. The presence of axial oxygens has proven crucial in allowing the present system to be doped with holes, despite the unusually large Cu–O in-plane distances. We note, however, that increased Ba substitution leads to enhanced 2D character of the systems, as both the in-plane Cu–O bond distances expand substantially to ~2.00 Å and the $CuO_6$ units become more severely elongated. This may lead to the fascinating possibility of successful electron-doping of the Ba-rich members along with hole-doping of the Sr-rich members of the series.

**Acknowledgment.** We thank SERC, EEC (Advanced Materials Programme), and BP for financial support of this work, the Institut Laue Langevin for provision of neutron time, and J. K. Cockcroft and C. Ritter for help with the experiments.

(15) Bertaut, E. F. *Acta Crystallogr. A* **1968**, *24*, 217.
(16) Vaknin, D.; Caignol, E.; Davies, P. K.; Fischer, J. E.; Johnston, D. C.; Goshorn, D. P. *Phys. Rev. B* **1989**, *39*, 9122.
(17) Tranquada, J. M.; Cox, D. E.; Kunnmann, W.; Moudden, H.; Shirane, G.; Suenaga, M.; Zolliker, P.; Vaknin, D.; Sinha, S. K.; Alvarez, M. S.; Jacobson, A. J.; Johnston, D. C. *Phys. Rev. Lett.* **1988**, *60*, 156.
(18) Shirane, G. *Acta Crystallogr.* **1959**, *12*, 282.
(19) Bacon, G. E. *Neutron Diffraction*; Clarendon Press: Oxford, U.K., 1975.
(20) We also note that the calculated intensities of the $(113)_M$ and $(115)_M$ magnetic reflections relative to the strongest $(111)_M$ reflection are at a minimum for $\mu \parallel c$. In $Sr_2CuO_2(CO_3)$, the ratio $I(113)/I(111)$ grows smoothly from 0.27 to 0.73 and $I(115)/I(111)$ from 0.07 to 0.44, as the angle that the spin direction makes with the unique axis $c$ changes from 0° to 90°.
(21) Two different samples with stoichiometry $Sr_{1.5}Ba_{0.5}CuO_2(CO_3)$ were examined, and the given magnetic moments represent the average value observed. For $Sr_{0.65}Ba_{1.35}CuO_2(CO_3)$, the presence of an impurity peak near the magnetic reflection precluded any quantitative estimates of the Cu magnetic moment for this sample.
(22) de Jongh, L. J.; Miedema, A. P. *Adv. Phys.* **1974**, *23*, 1.
(23) Chakravarty, S.; Halperin, B. I.; Nelson, D. R. *Phys. Rev. Lett.* **1988**, *60*, 1057.